Double ionization of He by ion impact: Second-order contributions to the fully differential cross section

S. D. López,[1,*] S. Otranto,[2] and C. R. Garibotti[1]
[1]*CONICET and Centro Atómico Bariloche, Avenida Bustillo Km 9.4, 8400 S. C. de Bariloche, Argentina*
[2]*IFISUR and Departamento de Física, Universidad Nacional del Sur, 8000 Bahía Blanca, Argentina*
(Received 25 March 2014; published 13 June 2014)

In this work, we present a second-order Born series treatment for the double ionization of He by ion impact. In particular, we show that the well-known independent events and independent electron models naturally result from an on-shell treatment for the second-order Born approximation. A transition amplitude which coherently includes first- and second-order terms in the projectile interaction is introduced to study the role of the two-step-1, shake-off, and two-step-2 mechanisms at different impact energies. Fully differential cross sections for proton and antiproton impact are presented and analyzed for different projectile momentum transfers.

DOI: 10.1103/PhysRevA.89.062709 PACS number(s): 34.50.Fa, 34.10.+x

I. INTRODUCTION

The calculation of cross sections for the atomic double ionization (DI) by ion impact provides a critical bench test for models aiming to describe the four-body dynamics in the continuum state. The situation differs from atomic single ionization by electron impact because for the usually tested He target, both outgoing electrons start from equivalent initial states, allowing for a simpler description of the process. During the last five decades, experiments have been conducted to study the process at the total cross-section level, from the pioneering work of Fedorenko [1] to the complete works of Shah *et al.* [2]. A comprehensive review of this topic was published in the 1980s by Dubois [3]. Now focusing on the underlying physics for this process, three collision mechanisms have been identified as responsible for the atomic DI at intermediate to large impact energies [4]. In the two-step-1 (TS-1) mechanism, alternatively denoted as knockout (KO), the projectile interacts with only one of the target electrons which subsequently ejects the other via the electron-electron interaction. In the shake-off (SO) mechanism, the second electron relaxes from an ionic bound state to continuum, following a sudden remotion of the primary electron. The third mechanism, usually referred to as two-step-2 (TS-2), considers that the electrons are ejected by two successive independent impacts by the projectile. In this case, the ionization of each electron is considered as an isolated event, independent of any subsequent or preceding atomic transition. The shake-off and TS-1 models involve one interaction of the projectile with a single electron and, therefore, could be described as first-order terms in a perturbative expansion of the scattering amplitude in the projectile charge (Z_P). In contrast, TS-2 involves two successive projectile-target interactions and hence its description requires a second-order term in Z_P [5]. At very high impact energies, the SO mechanism dominates the process and the initial-state correlation is relevant [5,6]. As the impact energy E decreases, the scattering event duration increases as well, and the electron-electron interaction should be expected to gain relevance throughout the whole process. No isolated mechanism is then expected to dominate the double-electron emission, and, in fact, a competition between the TS-2 and SO or TS-1 mechanisms has been reported [7–9].

At intermediate to large impact energies, independent electron emission approaches such as the independent electron (IEL) and the independent event (IEV) models provide a general description for the experimental atomic double-ionization total cross sections [10,11]. The IEL model considers that for a fast collision, the lapse between subsequent collisions is short enough so that both electrons are found in the same state [with the same ionization potential (IP)]. On the other hand, the IEV model considers that after the removal of the first electron, the second electron accommodates into the new ionic state, and the projectile needs to transfer an amount of energy equal to the vertical secondary IP to reach the double-electron emission. It has been observed that these models exhibit some dependence on the electron-electron correlation in the initial state. In contrast, the electron-electron final correlation gives a significant contribution to the DI total cross sections of He by impact of H^+ and He^{2+} ions, at intermediate energies [11,12]. This situation has been described by introducing in the IEL and IEV models the Coulomb density of states given by the Gamow factor that avoids the emission of electrons with the same momenta [11–14]. We note that the IEL and IEV models cannot be used to study (e,3e) processes, provided that the inherent straight-line trajectory approximation for the projectile does not apply.

While total cross sections for DI give insight into the process global trends, the fully differential cross sections (FDCS) provide the most detailed information on the collision process and on the electron correlation dynamics. A vast number of experimental and theoretical studies of the FDCS are found in the literature for atomic DI by electron impact [15,16]. Experiments have been mainly conducted by the group of Lahmam-Bennani, while several theoretical groups have worked during the last decade towards a successful description of their data [16–23]. We note that no theoretical model has yet been able to provide a full description of the data and several discrepancies have been reported throughout the years in what is still considered a challenging open field. On the other hand, experimental FDCS for atomic DI for ion impact are quite scarce [24]. These data have been obtained by means of the cold-target recoil-ion momentum spectroscopy (COLTRIMS) technique with relatively low resolution and are

*sebastian.lopez@cab.cnea.gov.ar

restricted to electrons with energies lower than 25 eV to avoid prohibitive extraction fields. In contrast, several theoretical studies can be found in the literature. Most of them are based on two- and three-body correlated wave functions and all of them rest on some sort of approximation throughout their numerical implementation [25–28]. The postcollisional interactions between the receding projectile and the emitted electrons have been incorporated via the introduction of effective charges [25,29]. Models based in four-body wave functions have been applied to the $(e,3e)$ process [30,31], but for DI by ion impact, the four-body dynamical coupling has only been accounted for using effective relative momenta [32]. Recently, with the Monte Carlo Event Generator tool, Ciappina *et al.* [33] have simulated the TS-2 mechanism from fully differential single-ionization cross sections [19].

In the first part of this paper, we focus on the physics of the TS-2 mechanism, which is expected to dominate at intermediate impact energies. In particular, we consider the DI of He atoms by proton impact, retaining second-order terms in the projectile charge [12]. A probabilistic TS-2 formalism was formerly applied to transfer ionization and double capture to the continuum [14,29]. We give a formal derivation of the TS-2 independent electron model starting from the four-body second order of a perturbative series for the scattering amplitude. A similar approach was already presented by Gravielle and Miraglia [34] for double-electron capture processes. We show that the resulting DI amplitude can be expressed as the convolution of two single-ionization amplitudes. These are calculated by means of the continuum distorted wave–eikonal initial state (CDW-EIS) theory of Crothers and McCann [35], which over the last three decades has led to reliable results for a large variety of projectiles and targets. Besides, this model represents, at intermediate impact energies, a clear improvement over the models based on the plane-wave initial state. We analyze the emitted electrons' angular distributions resulting from this second-order mechanism. Finally, we analyze a double-ionization scattering amplitude containing terms of first and second order in Z_P. In particular, we explore the relevance of the TS-2 and first-order mechanisms as the projectile momentum transfer varies, for proton and antiproton impact double ionization of He.

Atomic units ($e = m_e = \hbar = 1$) are used throughout this work, unless explicitly indicated.

II. A MODEL FOR THE TS-2 MECHANISM

The Hamiltonian of a system composed of a heliumlike target and an ionic and structureless projectile is

$$H = -\frac{1}{2\nu_T}\nabla^2_{R_T} + H_T + V_{P_1} + V_{P_2} + V_{PT}, \qquad (1)$$

where $\nu_T = mp(m_T + 2)/(m_P + m_T + 2)$ is the reduced mass of the projectile-target system, V_{P_i} is the Coulomb potential between the projectile and the electron i, and H_T is the atomic Hamiltonian:

$$H_T = -\frac{1}{2\mu_{T_1}}\nabla^2_{r_{T_1}} - \frac{1}{2\mu_{T_2}}\nabla^2_{r_{T_2}} + V_{T_1} + V_{T_2} + V_{12},$$

with $\mu_{Ti} = m_T m_i/(m_T + m_i)$ standing for the reduced mass of the electron i with respect to the target nucleus.

In a distorted-wave formalism, the transition amplitude is given by

$$T_{fi} = \langle \chi_f^- | T | \chi_i^+ \rangle \sim T_{fi}^{(1)} + T_{fi}^{(2)}, \qquad (2)$$

where

$$T_{fi}^{(1)} = \langle \chi_f^- | W_f^\dagger | \chi_i^+ \rangle; \quad T_{fi}^{(2)} = \langle \chi_f^- | W_f^\dagger G^+ W_i | \chi_i^+ \rangle. \qquad (3)$$

In this expression, $G^+ = (E - H + i\varepsilon)^{-1}$ is the total Green function, and surface terms are considered to be null. Here, χ_i^+ represents the initial distorted-wave function in which both electrons are bound to the target, and χ_f^- represents the final wave function for the two electrons in the continuum. These functions satisfy

$$(E - H \pm i\varepsilon)|\chi_{i,f}^\pm\rangle = -W_{i,f}|\chi_{i,f}^\pm\rangle.$$

While $T_{fi}^{(1)}$ consists of first-order mechanisms in terms of Z_P (i.e., TS-1 and SO), $T_{fi}^{(2)}$ includes second-order terms in Z_P which correspond to the two-step process (TS-2). Theoretical and experimental studies of double ionization of He by proton impact, at the total cross-section level, indicate that the TS-1 and SO mechanisms are small in comparison to the TS-2 at intermediate collision energies [8]. In contrast, at large impact energies, the SO mechanism turns dominant, clearly indicating a switch of roles among the physical mechanisms as the impact energy is varied.

In order to calculate $T_{fi}^{(2)}$, we expand the Green function in the base of its eigenfunctions,

$$G^+ = \sum_n |\psi_n\rangle \frac{1}{E - E_n + i\varepsilon}\langle\psi_n|, \qquad (4)$$

where $\{\psi_n\}$ spans the complete space of the four-body wave functions. This leads us to the following expression for the second-order terms:

$$T_{fi}^{(2)} = \sum_n \langle \chi_f^- | W_f^\dagger | \psi_n \rangle \frac{1}{E - E_n + i\varepsilon}\langle \psi_n | W_i | \chi_i^+ \rangle. \qquad (5)$$

Here, E_n are the eigenenergies of the four-body system.

Alternative ways to deal with this infinite summation have been proposed since the pioneering works of Massey and Mohr in the 1930s. This issue surfaced during the study of elastic scattering of electrons by atoms [36]. To make this expression tractable, these authors made use of the so-called closure approximation, in which E_n is replaced in the denominator of the Green function by an average energy $E_{\rm ave}$. This procedure provides a fast route to compute second-order terms,

$$\sum_n |\psi_n\rangle \frac{1}{E - E_n + i\varepsilon}\langle\psi_n| \sim \frac{1}{E - E_{\rm ave} + i\varepsilon}\sum_n |\psi_n\rangle\langle\psi_n|$$
$$= \frac{1}{E - E_{\rm ave} + i\varepsilon}. \qquad (6)$$

However, there is no precise procedure to choose $E_{\rm ave}$, and the outcome is usually very sensitive to the chosen value [20].

By the end of the 1960s, Holt and Moiseiwitsch [37] went beyond the closure approximation in their elastic electron-atom scattering studies. These authors evaluated the first two or three low-lying states of the summation exactly, and then used the closure approximation for the remaining terms.

Since then, many other ways to introduce superior orders have been developed. For instance, Garibotti and Massaro [38] variationally determined $E_{\rm ave}$ in order to evaluate the second-order term, and used the Padé approximants to compute the elastic scattering of electrons by atoms and compare their results with perturbative second-order calculations.

A decade later, Byron and Joachain [39] reported second-order calculations for atomic single ionization by electron impact within the closure approximation. In that work, they explored the sensitivity of the cross sections to the average energy considered, as well as the spread in the distributions this procedure originates. Other authors have kept up-to-date continuous track of this line of research for electron-atom collisions [40–43]. In the ion-atom single-ionization context, the development of the necessary set of tools to handle the second-order terms is much more recent. We can cite the works of Schulz [44], Voitkiv [45], and McGovern [46], among others. Nevertheless, we note that second-order terms were also studied in more complex problems: the works of Marchalant [47–49] and Fang [50] deal with excitation-ionization reactions, the work of Godunov [27] deals with transfer ionization reactions, and the work of Gravielle and Miraglia [34] addresses double capture.

For double ionization by electron impact, many authors have considered the second Born approximation [17–23]. In particular, for He targets, Dal Cappello *et al.* [20] have shown that the closure approximation drastically fails, since the mean energy has to be representative of states that range from -79 eV to the double continuum energy of an atom. Such an energy spread makes the closure approximation unreliable.

Another possibility is to express

$$\frac{1}{E-E_n+i\varepsilon}=P\left[\frac{1}{E-E_n+i\varepsilon}\right]-i\pi\delta(E-E_n),$$

and retain the on-shell contribution only [34,50]. This approximation is valid only if the numerator in Eq. (3) is a smooth function of the energy and contributions to the principal value from each side of the pole mutually cancel. In this case,

$$E=E_n=\frac{K_n^2}{2\nu_T}+\epsilon_{n1}+\epsilon_{n2}.$$

Here, ϵ_{n1} and ϵ_{n2} are the electronic energies when the system is found in the intermediate state, in which the electrons could be either bound or in the continuum. As the incident H^+ cannot be bound to the He atomic nucleus, the projectile remains, in the intermediate state, in a continuum state with momentum $\mathbf{K}_n$.

At this point, we can select diverse alternatives to deal with the sum over the intermediate states:

$$T_{fi}^{(2)}=-i\pi\sum_n\int d\mathbf{K}_n\langle\chi_f^-|W_f^\dagger|\psi_n\rangle\times\langle\psi_n|W_i|\chi_i^+\rangle\delta(E-E_n).\tag{7}$$

We now consider the subspace of the states $\{\xi_n\}\subset\{\psi_n\}$, composed of wave functions where the projectile is described by a distorted continuum wave of momentum $\mathbf{K}_n$, one electron is bound to the target, and the other is in the continuum with its final momentum $\mathbf{k}_n$. These states have an eigenenergy $E_n=E=\frac{K_n^2}{2\nu}+\frac{k_n^2}{2}+\epsilon_n$, where ϵ_n is the intermediate ion bound-state energy,

$$T_{fi}^{(2)}=-i\pi\sum_n\nu_T K_n\int d\Omega_n\langle\chi_f^-|W_f^\dagger|\psi_n\rangle\langle\psi_n|W_i|\chi_i^+\rangle.$$

From this equation, we can model the TS-2 mechanism by selecting only one intermediate state ξ_1, which provides the physical picture of one electron already emitted with final momentum $\mathbf{k}_1$ and the other still bound to the target. We observe that if we choose to represent the bound electron with a $He^+(1s)$ ground state, we are led to the independent event model (IEV). If we choose the He($1s$) bound electron instead, we are naturally led to the independent electron model (IEL). Then,

$$\begin{aligned}T_{fi}^{(TS-2)}(\mathbf{k}_1,\mathbf{k}_2,\Omega)&=\int d\Omega_n\langle\chi_f^-|W_f^\dagger|\xi_1\rangle\langle\xi_1|W_i|\chi_i^+\rangle\\&=\int d\Omega_n T_{fn}^{(1)}(\mathbf{K}_f-\mathbf{K}_n)T_{ni}^{(1)}(\mathbf{K}_n-\mathbf{K}_i).\end{aligned}\tag{8}$$

This amplitude is the convolution of two single-ionization amplitudes evaluated in a distorted-wave approximation. In this context, for χ_i^+ and χ_f^-, we choose the CDW-EIS approximation, for which $W_i=-\frac{\nabla_{r_P}^2}{2\mu_P}+\boldsymbol{\nabla}_{r_P}\cdot\boldsymbol{\nabla}_{r_T}$ and $W_f=-\boldsymbol{\nabla}_{r_P}\cdot\boldsymbol{\nabla}_{r_T}$.

We note that one of the transition amplitudes is in prior form, while the other is in post form. When the $\chi_{i,f}^+$ and the ψ_n functions correspond to the same potentials, there is no post-prior discrepancy. However, when approximate wave functions are recalled for which the potentials are not exactly the same, post-prior discrepancies arise and the present formulation of the IEV and IEL models might not be coincident with some earlier works, where simple products of probabilities were considered.

The FDCS are then written in terms of a symmetrized transition amplitude in order to account for the electrons indistinguishability,

$$\frac{d\sigma^{(TS-2)}}{d\mathbf{k}_1 d\mathbf{k}_2 d\Omega}=\frac{(2\pi)^4}{4v_i^2}\left|T_{fi}^{(TS-2)}(\mathbf{k}_1,\mathbf{k}_2,\Omega)+T_{fi}^{(TS-2)}(\mathbf{k}_2,\mathbf{k}_1,\Omega)\right|^2,$$

where $v_i=K_i/\nu_T$. We recall that we are evaluating the cross section retaining the TS-2 term only. This is equivalent to completely neglect the interelectronic interaction in the final state. However, nowadays it is recognized that the double-ionization process is sensitive to the electron-electron correlation even at intermediate energies. This means that even when the sequential interaction of the projectile with the electrons dominates the double-ionization process, the knockout mechanism must nevertheless be included [4]. A proper treatment for the whole problem must then contain an additional first-order term which could be given, in its simplest form, by the first Born approximation that we have derived in a former paper [25]. In the next section, we will analyze the results obtained by retaining the proposed TS-2 amplitude only, and, in the following one, we explicitly add a first-order term to provide an approximated complete model for the double-ionization problem.

III. EVALUATION OF THE AMPLITUDES AND RESULTS FROM THE TS-2 MODEL

In the CDW-EIS approximation, the initial wave function is given by

$$\chi_i(\mathbf{r}_{T1},\mathbf{r}_{T2},\mathbf{r}_{P1},\mathbf{r}_{P2}) = \phi(\mathbf{r}_{T1},\mathbf{r}_{T2})E_{-\mathbf{v}}(\mathbf{r}_{P1})E_{-\mathbf{v}}(\mathbf{r}_{P2}) \times e^{i\mathbf{K}_i.\mathbf{R}_{PT}}. \quad (9)$$

When using a central potential model, i.e., Hartree-Fock or configuration interaction expansions, the initial state $\phi_j(\mathbf{r}_{T1},\mathbf{r}_{T2})$ is given by a linear superposition of terms which are separable in the electrons coordinates:

$$\phi_j(\mathbf{r}_{T1},\mathbf{r}_{T2}) = \phi_j(\mathbf{r}_{T1})\phi_j(\mathbf{r}_{T2}).$$

In Eq. (9), $\mathbf{r}_{Tj}$ and $\mathbf{r}_{Pj}$ are the relative coordinates between the electron j and the target or projectile, respectively, and $\mathbf{R}_{PT}$ is the relative coordinate between the heavy particles. For ϕ_j, we use the monoelectronic wave functions tabulated by Clementi-Roetti [51].

The functions $E^{\pm}_{\mathbf{k}}(\mathbf{r})$ in Eq. (9) are the eikonal phases,

$$E^{\pm}_{\mathbf{k}}(\mathbf{r}) = e^{-i\alpha\ln(kr+\mathbf{k}.\mathbf{r})}.$$

On the other hand, the final state is given by

$$\chi_f(\mathbf{r}_{T1},\mathbf{r}_{T2},\mathbf{r}_{P1},\mathbf{r}_{P2}) = \psi_{\mathbf{k}_1}(\mathbf{r}_{T1})\psi_{\mathbf{k}_2}(\mathbf{r}_{T2})D_{\mathbf{k}_1-\mathbf{v}}(\mathbf{r}_{P1}) \times D_{\mathbf{k}_2-\mathbf{v}}(\mathbf{r}_{P2})e^{i\mathbf{K}_f.\mathbf{R}_{PT}}. \quad (10)$$

Here, $D^{\pm}_{\mathbf{k}}(\mathbf{r})$ represent the Coulomb distortion factors,

$$D^{\pm}_{\mathbf{k}}(\mathbf{r}) = \Gamma(1\pm i\alpha)e_1^{-\frac{\alpha\pi}{2}}F_1[\mp i\alpha,1,\pm i(kr\mp\mathbf{k}.\mathbf{r})], \quad (11)$$

and $\alpha = -Z_{P,T}/k$ is the Sommerfeld parameter.

In our present treatment, the intermediate state is expressed as follows:

$$\xi_1(\mathbf{r}_{T1},\mathbf{r}_{T2},\mathbf{r}_{P1},\mathbf{r}_{P2}) = \psi_{\mathbf{k}_1}(\mathbf{r}_{T1})\varphi(\mathbf{r}_{T2})D_{\mathbf{k}_1-\mathbf{v}_n}(\mathbf{r}_{P1}) \times E_{-\mathbf{v}_n}(\mathbf{r}_{P2})e^{i\mathbf{K}_n.\mathbf{R}_{PT}}, \quad (12)$$

with $\mathbf{v}_n = \mathbf{K}_n/v_T$.

The $\varphi(\mathbf{r}_{T2})$ in ξ_1 will be the ground state ($1s$) of the He atom or that of the He^+, depending upon whether we want to evaluate the double-ionization process with the IEL or the IEV model. The evaluation of the transition amplitude requires the integration over the coordinates of the two electrons. These integrals cannot be separated, requiring a full nine-dimensional integration. If we now neglect the eikonal distortion between the projectile and the passive electron, that is, $E_{-\mathbf{v}}(\mathbf{r}_{P2})$ and $E_{-\mathbf{v}_n}(\mathbf{r}_{P2})$ in $\langle\xi_1|W_i|\chi_i^+\rangle$, and $D_{\mathbf{k}_1-\mathbf{v}_n}(\mathbf{r}_{P1})$ and $D_{\mathbf{k}_1-\mathbf{v}}(\mathbf{r}_{P1})$ in $\langle\chi_f^-|W_f^\dagger|\xi_1\rangle$, the numerical complexity significantly reduces and we are led to the well-known CDW-EIS three-body transition amplitudes. Coulomb wave functions of charge 1.34 and 2.0 are used to represent the continuum states $\psi_{\mathbf{k}_{1,2}}(\mathbf{r}_{T1,2})$ for He and He^+, respectively.

From now on, we restrict our analysis to the double-electron emission along the collision plane (i.e., both electrons are emitted in the plane determined by the initial and final projectile momentum). In Fig. 1, we show a contour plot of the TS-2-FDCS as a function of the polar angles θ_1 and θ_2 of the emitted electrons taken from the incidence direction. The final projectile is scattered such that the momentum-transfer polar angle $\theta_Q \geqslant 0^\circ$. The presented FDCS correspond to double ionization of helium by protons impinging at 500 keV/amu, with both electrons emitted with $E_1 = E_2 = 10$ eV. In Figs. 1(a) and 1(b), we show the results obtained with the IEV and IEL models, respectively. Figures 1(c) and 1(d) retain the lines for these contours, which are superimposed over the recoil distribution to provide full access to the collision dynamics [25]. In this Figure we consider the threshold momentum transfer ($Q_{\text{threshold}} = 0.814$ a.u.). This is the configuration at which the momentum-transfer vector is parallel to the incident direction ($\theta_Q = 0$). This is the smallest momentum transfer that allows the emission of the two electrons and provides a physical picture of large-impact parameter collisions. This longitudinal momentum transfer can be expressed as follows:

$$Q_{\text{threshold}} = \Delta E/v_i, \quad \Delta E = \frac{k_1^2+k_2^2}{2} + I_o.$$

Here, $I_o = 79$ eV is the double-ionization energy for the He atom, and $I_o = I_1 + I_2$, where I_1 and I_2 are the energies required for the successive ionization of each electron. This energy is provided by the projectile,

$$K_f^2 = K_i^2 - v_T\left(k_1^2 + k_2^2 + 2I_1 + 2I_2\right).$$

In both models, the symmetrization imposed for the transition matrix for equal energy emission lead to axis-symmetric distributions along the main diagonal. In the IEV model, the sequential ionization energies $I_1 = 24.6$ eV and $I_2 = 54.4$ eV are considered, while in the IEL model, the first ionization energy $I_1 = 24.6$ eV is used for both electrons. As expected, double-electronic emission in the IEL model is described with an energy transfer of 49.2 eV instead of the real 79 eV, leading to larger double-ionization cross sections compared to the IEV model.

For the IEV model, we find a peak located near ($\theta_1 \approx -62^\circ$, $\theta_2 \approx 59^\circ$), in coincidence with a low value of the recoiling nucleus total momentum. This emission can be understood as two successive projectile-electron collisions, where in each collision one electron is emitted as in a single ionization with a maximum emission in the binary peak located in the direction of the partial momentum transfer, i.e., $\theta_{Q1} \sim \theta_1$. As the first ionization is from a He atom, the intermediate momentum of the projectile is given by

$$K_n^2 = K_i^2 - v\left(k_1^2 + 2I_1\right).$$

The momentum transfer Q_1 can be obtained from

$$K_n^2 = Q_1^2 - 2Q_1K_i\cos\theta_{Q1} + K_i^2.$$

The projectile scattering angles are of the order of 10^{-4} radians and we can safely assume that the projectile moves in a straight-line trajectory. By so doing, the present projectile momentum transfer is $Q_1 = 0.55$ a.u. We proceed in the same way for the second ionization, now from a He^+ ion, assuming $\theta_{Q2} \sim \theta_2$ to obtain $Q_2 = 1.08$ a.u. In these conditions,

$$\mathbf{Q}_{\text{threshold}} = \mathbf{Q}_1 + \mathbf{Q}_2.$$

A similar interpretation can be made for the symmetrical peak observed at ($\theta_1 \approx 59^\circ$, $\theta_2 \approx -62^\circ$).

Two additional structures can be observed in Fig. 1(a), located almost in opposite directions to the above-discussed peaks.

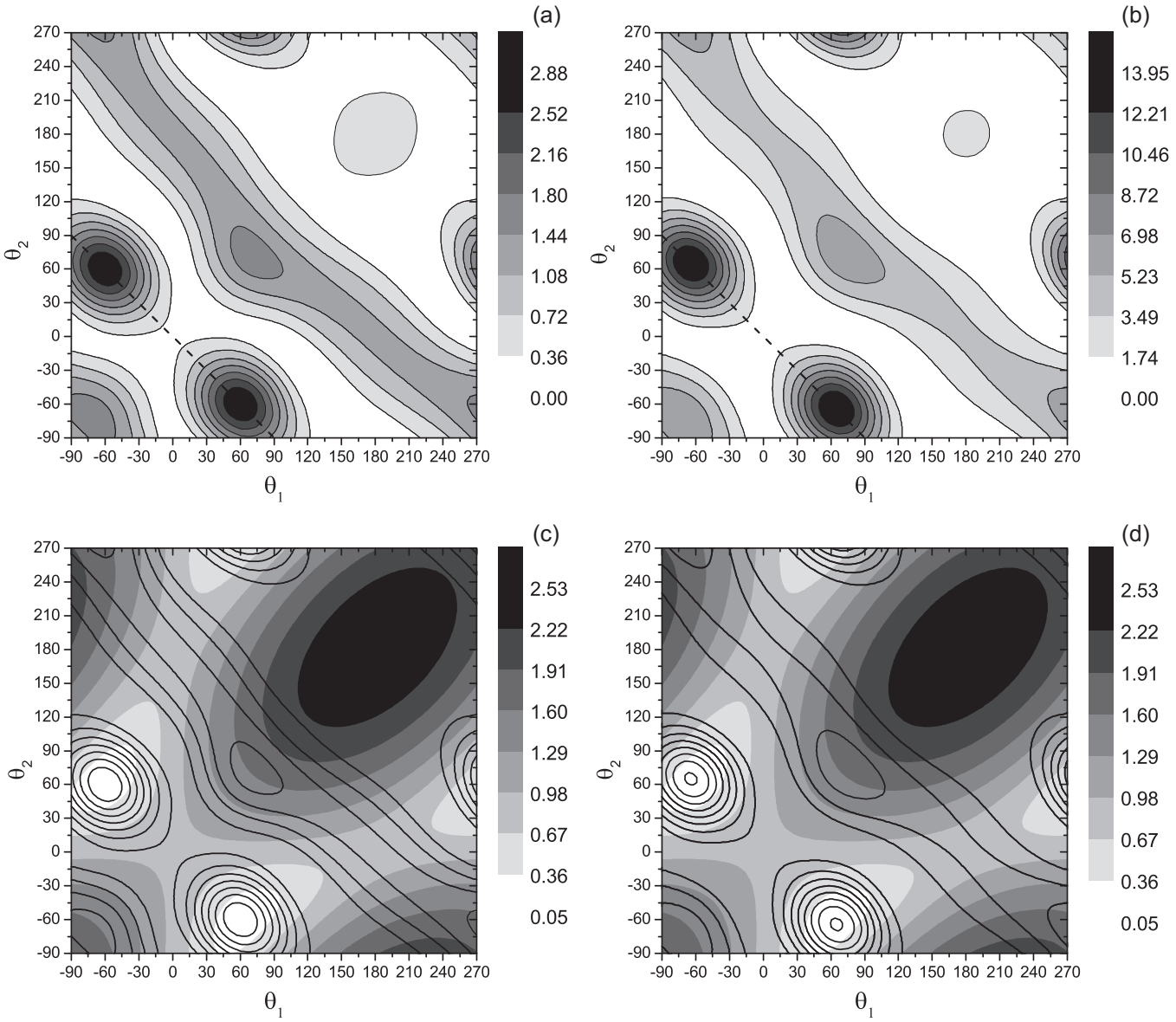

FIG. 1. Angular distributions of the FDCS (in terms of 10^{-6} a.u.) for DI of He by proton impact at 500 keV/amu. Both electrons are emitted with equal energy of 10 eV. The geometry chosen is coplanar. (a) Present IEV model. (b) Present IEL model. Recoil distributions (in a.u.) with FDCS as contour lines are shown in (c) and (d), respectively.

We note that the FDCS describe a coincidence event where the two electrons arrive simultaneously to detectors at different angles, and a maximum of the double-ionization FDCS will be observed after two successive single ionizations, when both are produced in angles of large emission. In single ionization, the angular distributions display two maxima, named binary and recoil peaks. Therefore, these new cusps can be considered as resulting from a binary collision of the projectile with one electron followed by a recoil-like collision with the second electron, and changing order for the other cusp. In both cusps, there is a relevant participation of the target nucleus, as can be observed in Figs. 1(c) and 1(d), where the respective FDCS are drawn over the recoil momentum contour plot [25].

The IEL case seems to show similar features as the IEV case, but now both collisions are equivalent and the maximum is observed at ($\theta_1 \approx -70^\circ$, $\theta_2 \approx -70^\circ$). A first inspection of Figs. 1(a) and 1(b) would suggest that both models behave similarly, though we notice that the maximums of the IEL have magnitudes nearly four times greater than those corresponding to the IEV model. This fact has been considered by many authors in the total cross-section context [11–13,52], and originates in the smaller value considered for the second electron ionization energy in the IEL model. In the following, we will no longer consider the IEL model because it does not present the correct energetic treatment.

In Fig. 2, we use the same collision energy as in Fig. 1, but we study the variation of the FDCS for the IEV model for unequal energy sharing between the electrons. The energy transferred to the electrons amounts to 50 eV, leading to $Q_{\text{threshold}} = 1.061$. The considered energy sharing for the electrons is $E_1 = E_2 = 25$, $E_1 = 30$, $E_2 = 20$ eV; and $E_1 = 40$, $E_2 = 10$ eV. The θ_1 angle corresponds to the fast electron

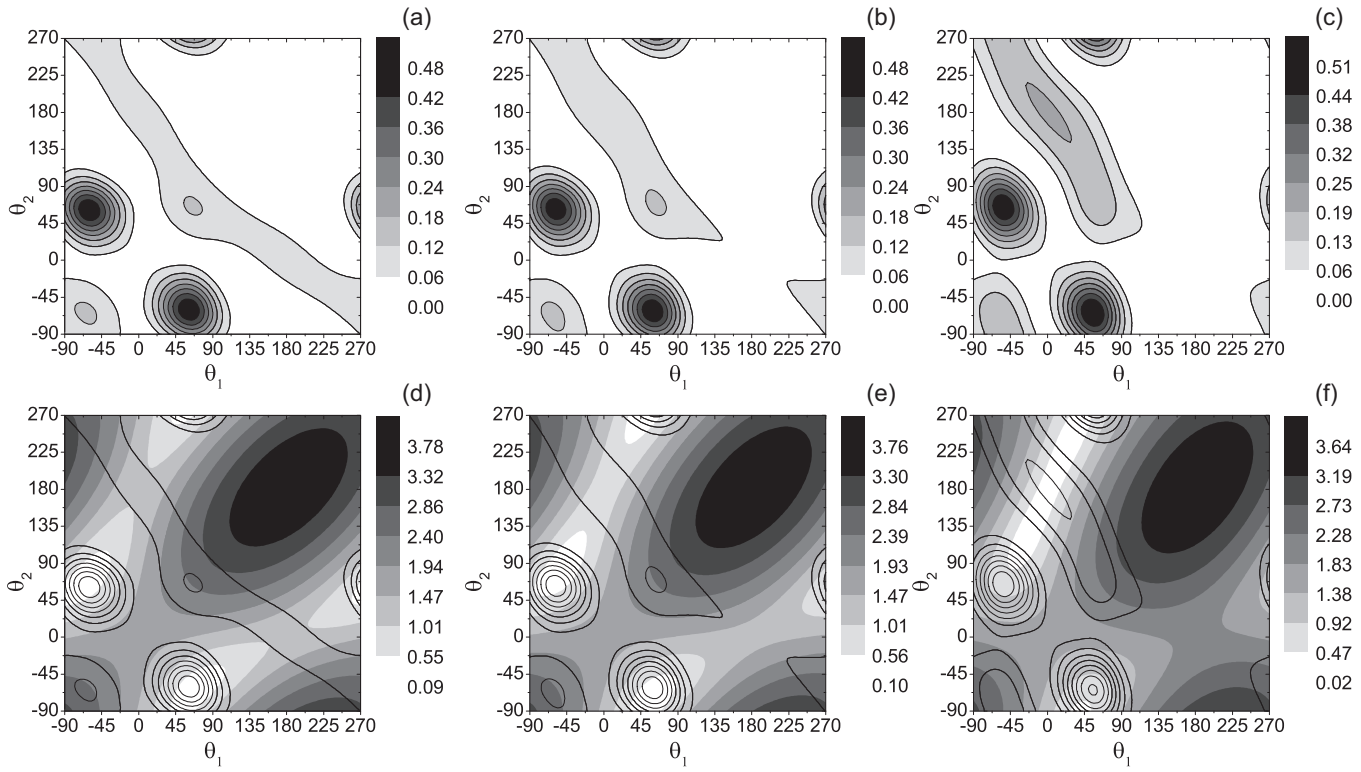

FIG. 2. Angular distributions of the FDCS (in terms of 10^{-6} a.u.) for DI of He by proton impact at 500 keV/amu. (a)–(c) Different energy sharing among the electrons is considered for the IEV model. The energies considered are (a),(d) $E_1 = E_2 = 25$ eV; (b),(e) E_1 =30 and $E_2 = 20$ eV; and (c),(f) E_1 =40 and $E_2 = 10$ eV. (d)–(f) Recoil distributions (in a.u.) with FDCS as contour lines for the IEV model.

and θ_2 corresponds to the slow one. The spectra exhibit a shape similar to Fig. 1, but now as the difference of energies between the electrons increases, the TS-2 collisions require a greater momentum transfer by the projectile. Furthermore, in Fig. 2(c), we observe the presence of antiparallel emission around $\theta_1 \approx 0^\circ$, $\theta_2 \approx 180^\circ$ [25]. In that case, the slow electron acquires a nearly isotropic distribution, and the fast electron originates in a hard collision with the projectile and is emitted in the forward quadrants only. This physical picture completes with the target core recoiling in the backward quadrants. The positions of the main lobes are slightly changed when the electron asymmetry energy is increased for a fixed total electronic energy, but now are located in a region where the recoil moment is relevant.

For antiproton impact, we have double-ionization mechanisms similar to those proposed for protons. However, the CDW-EIS amplitudes included in Eq. (3a) have different magnitudes, as will be discussed in the following section.

IV. CONTRIBUTION OF THE FIRST PERTURBATIVE ORDER

In earlier papers, we evaluated the FDCS from a scattering amplitude that includes a first-order projectile charge term in the perturbative Hamiltonian. We calculated the amplitude using a distorted-wave model that allowed the implementation of different wave functions for the initial and final states of the He subsystem.

The acting physical mechanisms in this first-order term in Z_P, i.e., SO and TS-1, involve the interaction of the projectile with only one electron. Subsequent interactions of the target atomic components lead to the double-electron emission. For SO, the fast removal of the primary electron by the projectile is followed by the emission of a slow secondary electron due to the sudden change of electronic screening. For TS-1, the primary electron knocks out the secondary electron in what can be considered a second-order collision for the primary electron. If expansions in terms of plane waves were recalled for the emitted electrons, a second-order term in the electron-electron interaction should be at least explicitly included to account for the TS-1 mechanism. However, when distorted waves (which incorporate infinite collision orders between particles) are used to represent the final state, the higher-order interactions are already included at the wave-function level.

Following [25], we write the first-order amplitude as

$$T_{fi}^{FBA}(\mathbf{k}_1,\mathbf{k}_2,\Omega) = \langle \chi_f^- | V_i | \chi_i^+ \rangle,$$

where

$$V_i = \frac{Z_P Z_T}{R} - \frac{Z_P}{|\mathbf{R}-\mathbf{r}_1|} - \frac{Z_P}{|\mathbf{R}-\mathbf{r}_2|}.$$

Here, $\mathbf{r}_1$ and $\mathbf{r}_2$ are the positions of the electrons relative to the target, $\mathbf{r}_{12} = \mathbf{r}_1 - \mathbf{r}_2$, and $\mathbf{R}$ is the distance between the ions. In the mentioned papers, we compare the electronic spectra resulting from two variational initial wave functions of different accuracy together with analytical wave functions proposed for the three-body continuum. The projectile is considered as a plane wave in both initial and final channels. Here we will apply the more elaborate model formerly developed, denominated DS3C. This corresponds to a correlated initial

state given by a Bonham and Kohl wave function (GS2) as adapted by Otranto *et al.* to avoid the introduction of spurious convergence factors in the evaluation of Nordsieck-like integrals [53]:

$$\chi_i^+(\mathbf{r}_1,\mathbf{r}_2) = \frac{1}{(2\pi)^{3/2}} e^{i\mathbf{K}_i\cdot\mathbf{R}} \psi_i^+(\mathbf{r}_1,\mathbf{r}_2),$$

with

$$\psi_i^+(\mathbf{r}_1,\mathbf{r}_2) = N_i(e^{-ar_1-br_2} + e^{-br_1-ar_2}) \times (e^{-z_c r_{12}} + C_0 e^{-\lambda r_{12}}), \quad (13)$$

where $N_i = 1.9358$, $a = 1.4126$, $b = 2.2068$, $\lambda = 0.199$, $C_0 = -0.6649$, and $z_c = 0.01$.

For the final state, we use the C3 wave function [54]:

$$\chi_f^- = \frac{1}{(2\pi)^{3/2}} e^{i\mathbf{K}_f\cdot\mathbf{R}} \psi_f^-, \quad (14)$$

and

$$\psi_f^-(\mathbf{k}_1,\mathbf{k}_2,\mathbf{r}_1,\mathbf{r}_2) = \frac{1}{(2\pi)^3}\frac{(1+P_{12})}{\sqrt{2}}[e^{i(\mathbf{k}_1\cdot\mathbf{r}_1+\mathbf{k}_2\cdot\mathbf{r}_2)} D_{\mathbf{k}_1}(\eta_1,\mathbf{r}_1) \times D_{\mathbf{k}_2}(\eta_2,\mathbf{r}_2) D_{\mathbf{k}_{12}}(\eta_{12},\mathbf{r}_{12})], \quad (15)$$

where P_{12} is the permutation operator and $D_{\mathbf{k}}(\eta,\mathbf{r})$ is the Coulomb distortion factor given by Eq. (11).

The C3 model entirely considers the interactions between the three charged particles but assumes static charges that do not account for the dynamical screening produced by the relative motion of the four particles in the final state. The dynamical screening model, DS3C, introduces effective charges to consider the dynamical correlation between the electrons and the target nucleus [55]. In this case, the Sommerfeld parameters are given by $\eta_1 = Z^{DS}_{e_1-\mathrm{He}^+}/k_1$, $\eta_2 = Z^{DS}_{e_2-\mathrm{He}^+}/k_2$, and $\eta_{12} = Z^{DS}_{e_1-e_2}/(2k_{12})$ with $\mathbf{k}_{12} = (\mathbf{k}_1 - \mathbf{k}_2)/2$. The explicit expression of the effective charges can be found in our earlier paper [25], where we compare the double-emission electronic spectra resulting from different models for the two-electron continuum, in particular the DS3C.

With these functions, the electron-electron interaction is introduced in the initial and final state. Even when the separation between the shake-off and TS-1 mechanisms is not explicit, both mechanisms are inherently included at the wave-function level.

The double-ionization amplitude, up to second order, remains

$$T_{fi} = T_{fi}^{FBA}(\mathbf{k}_1,\mathbf{k}_2,\Omega) + \tfrac{1}{2}\left[T_{fi}^{(TS-2)}(\mathbf{k}_1,\mathbf{k}_2,\Omega) + T_{fi}^{(TS-2)}(\mathbf{k}_2,\mathbf{k}_1,\Omega)\right] \quad (16)$$

and

$$\frac{d\sigma}{d\mathbf{k}_1 d\mathbf{k}_2 d\Omega} = \frac{(2\pi)^4}{v_i^2}\left| T_{fi}^{FBA}(\mathbf{k}_1,\mathbf{k}_2,\Omega) + \frac{1}{2}[T_{fi}^{(TS-2)}(\mathbf{k}_1,\mathbf{k}_2,\Omega) + T_{fi}^{(TS-2)}(\mathbf{k}_2,\mathbf{k}_1,\Omega)]\right|^2. \quad (17)$$

Therefore, the FDCS will contain Z_P^2, Z_P^3, and Z_P^4 terms.

Now we will consider the dependence of the electrons' angular distribution as the momentum transfer increases, for the same collision geometry, impact energy, and electrons emission energies considered in Fig. 1. In the first row of Fig. 3, we display the electronic distributions for double ionization of He atoms by proton impact, for $Q = 1.0$, 1.5, and 3 a.u. resulting from the first Born approximation (FBA); in the second row, we display the IEV model; and, in the third row, we show the coherent sum of the FBA plus IEV amplitudes, as given by Eq. (16). The successive columns correspond to increasing values of Q. In the FDCS given by the FBA, for equal energy emission, the main features have been thoroughly described in an earlier paper [56]. In the contour-plot representation, the momentum-transfer direction is fixed. From the momentum conservation law $\mathbf{Q} = \mathbf{k}_1 + \mathbf{k}_2 + \mathbf{R}$, we can distinguish three main structures in the angular distributions given by the FBA that are characterized by the particular values of the momentum R acquired by the recoiling nucleus once the collision has taken place. These structures are usually denoted as the *binary* and the *recoil* peaks, for which the electrons' momenta are located along the dashed lines drawn in each plot of Fig. 3 [56] axially symmetric in relation to the Q direction. In the *binary* emission, the total electronic momentum is similar to the momentum transfer $\mathbf{k}_1 + \mathbf{k}_2 \approx \mathbf{Q}$, and the recoil ion is mainly a spectator during the collision ($R \approx 0$). The projectile transfers the momentum to one electron which then hits the second one. In this picture, both electrons are emitted in quasiorthogonal directions, while the nucleus remains almost still. This mechanism, where the target remains as a spectator, as in the binary collision in single ionization, is denoted as the two-step 1 (TS-1) process [16]. In the *recoil* emission, the total momentum of the electrons has the same magnitude but is opposite to the momentum transfer ($\mathbf{k}_1 + \mathbf{k}_2 \approx -\mathbf{Q}$), therefore $\mathbf{R} \approx 2\mathbf{Q}$. The projectile hits one electron which is scattered backwards by the nucleus, and this electron knocks the other one before leaving the atom. The electrons leave the reaction zone with a relative angle equal to 90°, and the repulsion between the electrons increases this angle. Another structure we observe is produced by the *back-to-back emission*, where the electrons are ejected in opposite directions ($\mathbf{k}_1 + \mathbf{k}_2 \approx 0$) with $\mathbf{R} \approx \mathbf{Q}$. This structure can be explained in terms of successive classical collisions considering that the projectile hits one electron and this electron hits the nucleus going backwards with $\mathbf{k}_1 \approx -\mathbf{Q}$. The nucleus then recoils with $\mathbf{R} \approx 2\mathbf{Q}$ and hits the other electron, which acquires a momentum $\mathbf{k}_2 \approx \mathbf{Q}$.

Finally, it should be taken into account that as the momentum transfer increases, the role played by the target nucleus during the collision process increases and the complexity of the double-emission process increases as well.

For the DS3C model, a shift from strictly orthogonal emission arises because the momenta exchanges between the three particles are allowed by the model via the effective charges, and, on the other hand, by the repulsion among the electrons. In Fig. 3(a), these features are easier to locate, being the *binary* structure centered at ($\theta_1 \approx -5°$, $\theta_2 \approx 70°$), while the *recoil* structure is located at ($\theta_1 \approx 160°$, $\theta_2 \approx 250°$).

Concerning the SO mechanism, in which one of the electrons acquires the projectile momentum transfer while the other relaxes to the continuum isotropically, it is expected to be relevant for very asymmetric geometries for which the sudden approximation turns valid. In a recent paper, we have shown that signatures of the SO mechanism can be identified

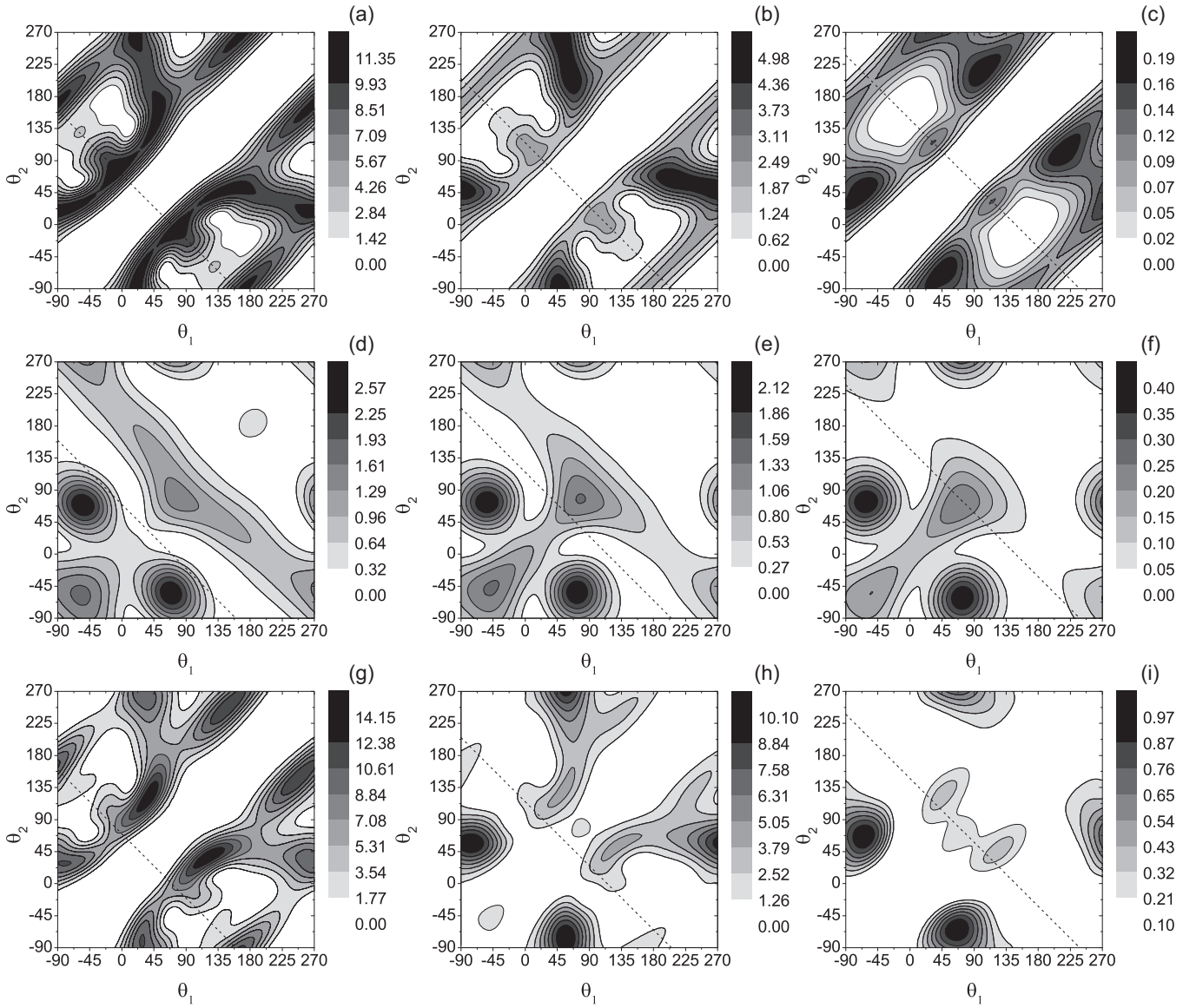

FIG. 3. Angular distributions of the FDCS (in terms of 10^{-6} a.u.) for DI of He by proton impact at 500 keV/amu. Both electrons emitted with 10 eV each. Three momentum transfer magnitudes are considered: (a),(d),(g) $Q = 1$ a.u.; (b),(e),(h) $Q = 1.5$ a.u.; and (c),(f),(i) $Q = 3$ a.u. (a)–(c) The first row corresponds to calculations performed with the FBA, (d)–(f) the second row corresponds to calculations performed with the present IEV model, and (g)–(i) the third row corresponds to the coherent sum of both terms. The dotted lines in each panel indicate the electronic polar angles θ_1 and θ_2 for which $\mathbf{k}_1 + \mathbf{k}_2$ are parallel to $\mathbf{Q}$.

in the angular distributions corresponding to double-electron emissions in which one of the electrons is fast, while the other is rather slow [25]. Clearly, these two mechanisms cannot be isolated within the DS3C model. However, their separate contributions can be eventually tested by switching on and off the initial-state correlation or the interelectronic interaction in the final state [57].

For Q near $Q_{\text{threshold}}$, the FBA is larger than the IEV, but as Q increases, the magnitude of the FDCS given by the FBA decreases faster than that obtained with the IEV model. This is a consequence of the increased probability for a large momentum transfer after two successive projectile-electron collisions. In addition, we note that the recoiling nucleus acquires a major role in the collision. This behavior is clearly evident in the last row of Fig. 3, where we clearly note that the TS-2 mechanism becomes dominant for large Q. For equal energy electrons, a signature of second- or higher-order processes is a breakup of the symmetry of the cross section with respect to Q.

The FBA remains symmetric along the momentum-transfer directions, which are $\theta_Q \approx 35^\circ$ for $Q = 1.0$ a.u., $\theta_Q \approx 57^\circ$ for $Q = 1.5$ a.u., and $\theta_Q \approx 74^\circ$ for $Q = 3.0$ a.u. Meanwhile, as Q increases, the distributions given by the IEV model present similar features to the threshold case, and the maximums remain almost at the same position. As a result, the FDCS resulting from the full second order is not symmetric along Q [58].

In Fig. 4, we show the electronic distributions for double ionization of He atoms by antiproton impact, for the same conditions as in Fig. 3. The FBA distributions are equal to

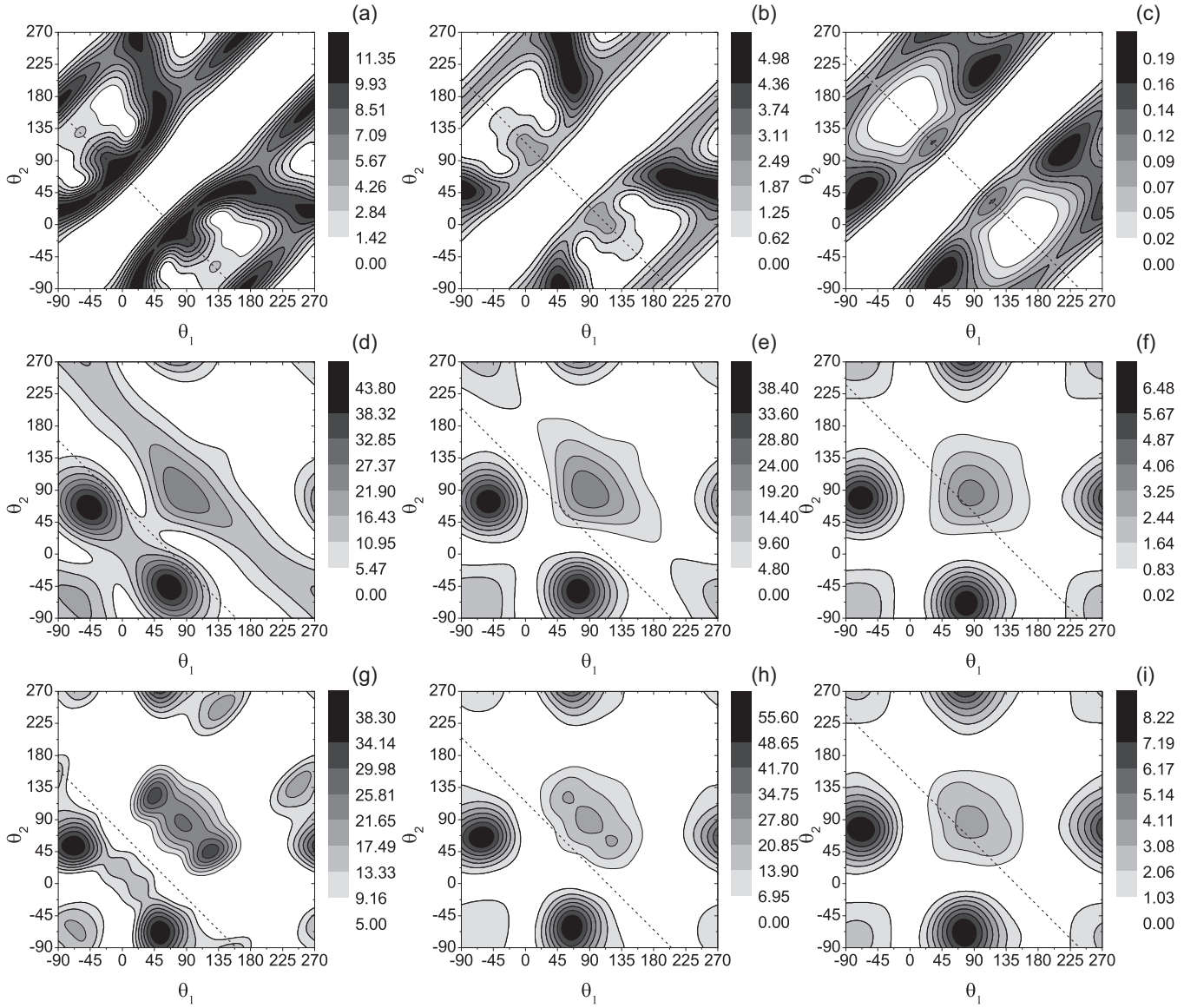

FIG. 4. Angular distributions of the FDCS (in terms of 10^{-6} a.u.) for DI of He by antiproton impact at 500 keV/amu. Both electrons emitted with 10 eV each. Three momentum-transfer magnitudes are considered: (a),(d),(g) $Q = 1$ a.u.; (b),(e),(h) $Q = 1.5$ a.u.; and (c),(f),(i) $Q = 3$ a.u. (a)–(c) The first row corresponds to calculations performed with the FBA, (d)–(f) the second row corresponds to calculations performed with the present IEV model, and (g)–(i) the third row corresponds to the coherent sum of both terms.

those represented in Fig. 3; therefore we only show the FDCS calculated with the IEV model and those resulting from the corresponding full amplitude [Eq. (16)]. The shapes of the IEV distributions are similar to those obtained for proton impact. However, their magnitudes are almost 20 times larger, probably due to the strongest repulsion between the negatively charged particles. The interference between the first and the second order reduces the difference in the complete FDCS, which is dominated by the TS-2 mechanism even at low values of Q.

V. CONCLUSIONS

We have given a formal derivation of the TS-2 mechanism starting from a second-order perturbative expansion for the double-ionization scattering amplitude in terms of the projectile charge. Via an on-shell treatment for these second-order terms, we have provided a consistent theoretical description of the IEV and IEL models usually recalled *ad hoc* as products of probabilities. Complementing our earlier works based on a first-Born-approximation-type treatment, in this work we have introduced an approximated transition amplitude which coherently incorporates the TS-2 information via an on-shell treatment of the second-Born-approximation terms. The angular distributions of the electrons resulting from the double ionization of He by proton or antiproton impact present structures that can be associated to two independent collisions by the projectile. In the IEV formalism, when the momentum transfer of the projectile is given by the DI threshold value ($Q_{\text{threshold}}$), and for equal velocity electrons, the main peaks observed in the angular distributions can be associated to two independent single ionizations. These peaks are located along the line where $\theta_1 + \theta_2 \sim \theta_Q$, which indicate a binary DI. For

Q values larger than $Q_{\text{threshold}}$, the peaks almost conserve their positions and lose correlation with the direction of the momentum transfer. In this case, the target core must always absorb a recoil momentum and a net binary DI is not possible. This is a strong difference from the results given by the first Born approximation, where the angular structures of the FDCS rotate as long as **Q** changes its direction. The sum of the FBA and the IEV amplitude allowed us to write a double-ionization amplitude containing all of the main physical mechanisms in the process. For proton impact and threshold projectile momentum transfers, we found that the FBA dominates and the maximum emission is along the direction of Q, presenting the *binary* and *recoil* peaks. As Q increases, the TS-2 contribution dominates and the maximum emission corresponds to the situation where the projectile undergoes independent collisions with each electron. For antiproton impact, the magnitude of the FDCS is larger than in the proton case and the IEV features dominate over all the range of Q. It would be highly desirable if new experimental data were available in the near future to help us refine our understanding of the double-electron emission at a differential level.

ACKNOWLEDGMENTS

This work was supported by Grants No. PIP 112-201101-00749 of CONICET and No. PGI 24/F059 of UNS, Argentina.

[1] N. V. Fedorenko, Sov. Phys. Usp. **2**, 526 (1959).
[2] M. B. Shah and H. B. Gilbody, J. Phys. B **18**, 899 (1985).
[3] R. D. DuBois and S. T. Manson, Phys. Rev. A **35**, 2007 (1987).
[4] H. Knudsen, L. H. Andersen, P. Hvelplund, G. Astner, H. Cederquist, H. Danared, L. Liljeby, and K.-G. Rensfelt, J. Phys. B **17**, 3545 (1984).
[5] J. H. McGuire, Phys. Rev. Lett. **49**, 1153 (1982).
[6] J. F. Reading and A. L. Ford, Phys. Rev. Lett. **58**, 543 (1987).
[7] J. McGuire, *Electron Correlation Dynamics in Atomic Collisions*, Cambridge Monographs on Atomic, Molecular and Chemical Physics (Cambridge University Press, New York, 2005).
[8] J. H. McGuire, Adv. At. Mol. Opt. Phys. **29**, 217 (1991).
[9] A. L. Godunov, J. H. McGuire, V. S. Schipakov, H. R. J. Walters, and C. T. Whelan, J. Phys. B **39**, 987 (2006).
[10] D. S. F. Crothers and R. McCarroll, J. Phys. B **20**, 2835 (1987).
[11] M. McCartney, J. Phys. B **30**, L155 (1997).
[12] L. Gulyás, A. Igarashi, P. D. Fainstein, and T. Kirchner, J. Phys. B **41**, 025202 (2008).
[13] M. Fiori, A. B. Rocha, C. E. Bielschowsky, G. Jalbert, and C. R. Garibotti, J. Phys. B **39**, 1751 (2006).
[14] L. Gulyás, A. Igarashi, and T. Kirchner, Phys. Rev. A **86**, 024701 (2012).
[15] A. Lahmam-Bennani, C. Dupre, and A. Duguet, Phys. Rev. Lett. **63**, 1582 (1989).
[16] A. Dorn, A. Kheifets, C. D. Schröter, B. Najjari, C. Höhr, R. Moshammer, and J. Ullrich, Phys. Rev. A **65**, 032709 (2002).
[17] A. Lahmam-Bennani, A. Duguet, C. Dal Cappello, H. Nebdi, and B. Piraux, Phys. Rev. A **67**, 010701 (2003).
[18] A. S. Kheifets, Phys. Rev. A **69**, 032712 (2004).
[19] E. M. Staicu Casagrande, C. Li, A. Lahmam-Bennani, C. Dal Cappello, M. Schulz, and M. Ciappina, J. Phys. B **44**, 055201 (2011).
[20] C. Dal Cappello, A. Haddadou, F. Menas, and A. C. Roy, J. Phys. B **44**, 015204 (2011).
[21] A. Mansouri, C. Dal Cappello, S. Houamer, I. Charpentier, and A. Lahmam-Bennani, J. Phys. B **37**, 1203 (2004).
[22] C. Dal Cappello, C. Champion, I. Kada, and A. Mansouri, Phys. Rev. A **83**, 062716 (2011).
[23] C. Li, A. Lahmam-Bennani, E. M. Staicu Casagrande, and C. Dal Cappello, J. Phys. B **44**, 115201 (2011).
[24] D. Fischer, R. Moshammer, A. Dorn, J. R. Crespo López-Urrutia, B. Feuerstein, C. Höhr, C. D. Schröter, S. Hagmann, H. Kollmus, R. Mann, B. Bapat, and J. Ullrich, Phys. Rev. Lett. **90**, 243201 (2003).
[25] S. D. López, C. R. Garibotti, and S. Otranto, Phys. Rev. A **83**, 062702 (2011).
[26] M. F. Ciappina, M. Schulz, T. Kirchner, D. Fischer, R. Moshammer, and J. Ullrich, Phys. Rev. A **77**, 062706 (2008).
[27] A. L. Godunov, C. T. Whelan, and H. R. J. Walters, Phys. Rev. A **78**, 012714 (2008).
[28] E. M. Lobanova, S. A. Sheinerman, and L. G. Gerchikov, Sov. J. Exper. Theor. Phys. **105**, 486 (2007).
[29] L. Gulyás, L. Sarkadi, A. Igarashi, and T. Kirchner, Phys. Rev. A **82**, 032705 (2010).
[30] J. R. Götz, M. Walter, and J. S. Briggs, J. Phys. B **39**, 4365 (2006).
[31] J. Berakdar, Phys. Rev. A **55**, 1994 (1997).
[32] S. D. López, S. Otranto, and C. R. Garibotti, Phys. Rev. A **87**, 022705 (2013).
[33] M. F. Ciappina, T. Kirchner, and M. Schulz, Comput. Phys. Commun. **181**, 813 (2010).
[34] M. S. Gravielle and J. E. Miraglia, Phys. Rev. A **45**, 2965 (1992).
[35] D. S. F. Crothers and J. F. McCann, J. Phys. B **16**, 3229 (1983).
[36] H. S. W. Massey and C. B. O. Mohr, R. Soc. London Proc. Ser. A **146**, 880 (1934).
[37] A. R. Holt and B. L. Moiseiwitsch, J. Phys. B **1**, 36 (1968).
[38] C. R. Garibotti and P. A. Massaro, J. Phys. B **4**, 79 (1971).
[39] F. W. Byron, Jr., C. J. Joachain, and B. Piraux, J. Phys. B **13**, L673 (1980).
[40] F. W. Byron, Jr., C. J. Joachain, and B. Piraux, J. Phys. B **15**, L293 (1982).
[41] F. W. Byron, Jr., C. J. Joachain, and B. Piraux, J. Phys. B **16**, L769 (1983).
[42] C. Dal Cappello, I. Charpentier, S. Houamer, P. A. Hervieux, M. F. Ruiz-Lopez, A. Mansouri, and A. C. Roy, J. Phys. B **45**, 175205 (2012).
[43] C. Dal Cappello, B. Hmouda, A. Naja, and G. Gasaneo, J. Phys. B **46**, 145203 (2013).
[44] M. Schulz, R. Moshammer, D. H. Madison, R. E. Olson, P. Marchalant, C. T. Whelan, H. R. J. Walters, S. Jones, M. Foster, H. Kollmus, A. Cassimi, and J. Ullrich, J. Phys. B **34**, L305 (2001).
[45] A. B. Voitkiv, B. Najjari, and J. Ullrich, J. Phys. B **36**, 2591 (2003).
[46] M. McGovern, C. T. Whelan, and H. R. J. Walters, Phys. Rev. A **82**, 032702 (2010).

[47] P. J. Marchalant, C. T. Whelan, and H. R. J. Walters, J. Phys. B **31**, 1141 (1998).
[48] P. J. Marchalant, J. Rasch, C. T. Whelan, D. H. Madison, and H. R. J. Walters, J. Phys. B **32**, L705 (1999).
[49] P. J. Marchalant, B. Rouvellou, J. Rasch, S. Rioual, C. T. Whelan, A. Pochat, D. H. Madison, and H. R. J. Walters, J. Phys. B **33**, L749 (2000).
[50] Y. Fang and K. Bartschat, J. Phys. B **34**, L19 (2001).
[51] E. Clementi and C. Roetti, At. Data Nucl. Data Tables **14**, 177 (1974).
[52] J. Bradley, R. J. S. Lee, M. McCartney, and D. S. F. Crothers, J. Phys. B **37**, 3723 (2004).
[53] S. Otranto, G. Gasaneo, and C. R. Garibotti, Nucl. Instrum. Methods Phys. Res. B **217**, 12 (2004).
[54] C. R. Garibotti and J. E. Miraglia, Phys. Rev. A **21**, 572 (1980).
[55] J. Berakdar, Phys. Rev. A **53**, 2314 (1996).
[56] S. D. López, C. R. Garibotti, and S. Otranto, Nucl. Instrum. Methods Phys. Res. B **283**, 63 (2012).
[57] Z.-J. Teng and R. Shakeshaft, Phys. Rev. A **49**, 3597 (1994).
[58] A. Lahmam-Bennani, E. M. Staicu Casagrande, A. Naja, C. Dal Cappello, and P. Bolognesi, J. Phys. B **43**, 105201 (2010).